Contents

1 Introduction **1**
- 1.1 The radio sky . . . 1
- 1.2 Active galaxies and the standard model of AGN . . . 3
  - 1.2.1 The zoo of active galaxies . . . 3
  - 1.2.2 Basic ingredients of an AGN . . . 5
  - 1.2.3 The unified scheme . . . 8
- 1.3 A small gallery of radio and X-ray jets . . . 8
  - 1.3.1 Kiloparsec–scale radio and X-ray jets . . . 8
  - 1.3.2 Parsec–scale radio jets . . . 11
- 1.4 NGC 1052 – The star of the show . . . 13

2 Theoretical background **21**
- 2.1 Synchrotron radiation . . . 21
  - 2.1.1 Emission mechanism . . . 21
  - 2.1.2 Spectral distribution . . . 22
  - 2.1.3 The SSC mechanism . . . 23
- 2.2 Jets . . . 24
  - 2.2.1 Jet formation and propagation . . . 24
  - 2.2.2 Jet emission . . . 26
  - 2.2.3 The core–shift . . . 26

3 Observations and data reduction **31**
- 3.1 Fundamentals of radio aperture synthesis . . . 31
- 3.2 Observations of NGC 1052 with the VLBA . . . 33
- 3.3 VLBI data reduction . . . 34

4 Results **49**
- 4.1 Total intensity mapping . . . 49
- 4.2 Model fitting and image alignment . . . 52
- 4.3 Spectral analysis . . . 58
- 4.4 Brightness temperature distribution . . . 70
- 4.5 Polarimetry . . . 76
- 4.6 Core shift analysis . . . 81

5 The big picture **83**

List of Figures

1.1 The radio sky at 408 MHz . . . 2
1.2 Optical spectra of a Seyfert 2 galaxy and a LINER . . . 5
1.3 Sketch of the standard model . . . 7
1.4 Six examples of jets on VLA scales . . . 10
1.5 Cygnus A at radio and X-ray wavelengths . . . 12
1.6 Six examples of pc–scale radio jets taken from the VLBA 2 cm survey . . . 14
1.7 The emission cone in Hα of NGC 1052 and its optical jet . . . 16
1.8 The pc–scale twin jet in NGC 1052 at 22 GHz . . . 18

2.1 Dependence of jet parameters on pressure gradients . . . 28

3.1 An elementary radio interferometer . . . 32
3.2 The antennas of the VLBA . . . 34
3.3 A POSSM plot of one scan after the fringe fitting . . . 37
3.4 The basic path of data *a–priori* calibration in $\mathcal{AIPS}$. . . . 38
3.5 A (u, v)–plot, showing the location of baselines in the (u, v)–plane during the 43 GHz observation of NGC 1052 . . . 39
3.6 Time coverage of the NGC 1052 observation at 43 GHz. . . . 40
3.7 The 43 GHz visibility versus time of the *a–priori* calibrated and the fully edited and self–calibrated data on the baseline FD–PT. . . . 42
3.8 The visibility distribution projected on two perpendicular planes in the (u, v)–plane . . . 42
3.9 Fourier relationship between the brightness and visibility amplitude at 5 GHz 44
3.10 The basic feed self–calibration path in $\mathcal{AIPS}$. . . . 48

4.1 Contour plots of the total intensity flux of NGC 1052 at the observed frequencies . . . 50
4.2 Locations of the various model components on the sky . . . 57
4.3 The aligned model fit maps. . . . 59
4.4 The aligned CLEAN maps. . . . 60
4.5 Spectral index map between 5 and 8.4 GHz . . . 62
4.6 Spectral index map between 8.4 and 22 GHz . . . 63
4.7 Spectral index map between 22 and 43 GHz . . . 64
4.8 Total spectrum of the pc-scale structure of NGC 1052 . . . 65
4.9 The spectra of the four jet regions A,B,C and D. . . . 67
4.10 Spectra of the model fit components in the eastern jet . . . 68
4.11 Spectral indices of the model components . . . 69

4.12 The jet-to-counterjet ratio determined from the fluxes of the model fit components as a function of frequency 70
4.13 Logarithmic representation of the brightness temperature distribution along the eastern jet of NGC 1052 72
4.14 Frequency dependence of the brightness temperatures in the eastern jet of NGC 1052 75
4.15 Calculated opacities along the eastern jet of NGC 1052 77
4.16 Polarized emission images of 3C 345 at 5, 8.4, 22 and 43 GHz 78
4.17 Map of the polarized emission in NGC 1052 at 5 GHz 79
4.18 Slice through the total intensity and polarized emission along the eastern jet of NGC 1052 at 5 GHz. 80
4.19 Image with the model fitting results of the 43 GHz data 81
4.20 Core positions in the two jets at the different frequencies 82

5.1 Model of the central parsecs in NGC 1052 85

Chapter 2

Theoretical background

In this chapter theoretical background necessary for the proper understanding of the following chapters is presented. In section 2.1 the basic principles of synchrotron emission are discussed and some fundamental equations for the description of a synchrotron emitting source are derived. Especially relativistic effects will be taken into account and a possible connection between radio and X-ray spectra is investigated, the SSC mechanism. Section 2.2 will deal with synchrotron emission from jets in special consideration of the frequency dependence of the jet-core location.

2.1 Synchrotron radiation

2.1.1 Emission mechanism

Whenever a charged particle passes a region with an electromagnetic field it will interact with this field encountering the Lorentz force

$$\vec{F_L} = q\left(\vec{E} + \vec{\beta} \times \vec{B}\right) \tag{2.1}$$

with $\vec{\beta} = \vec{v}/c$, the velocity in units of the speed of light and q, the charge of the particle. In the case of a vanishing electric field ($\vec{E} = 0$) it will be accelerated perpendicularly to the magnetic field $\vec{B}$. For a linear magnetic field this will result in a helical motion around the direction of $\vec{B}$ as a superposition of a constant velocity component along the field and a constant acceleration perpendicular to it. It will orbit with a period $\gamma mc/2\pi qB$ corresponding to the Larmor frequency

$$\omega_B = \frac{qB}{\gamma mc} \tag{2.2}$$

with the Lorentz factor $\gamma = 1/\sqrt{1-\beta^2}$ and the mass m of the particle. In the non-relativistic case (Cyclotron radiation) the particle will emit an electromagnetic wave with this frequency. It can be shown that the emitted power for each electron energy is given by

$$P = 4/3\,\sigma_T\,c\,(\gamma\beta)^2\,U_B \propto \gamma^2 U_B \tag{2.3}$$

(Larmor formula, see Rybicki & Lightman 1979 for details), with $\sigma_T = 8\pi e^4/m^2c^4$, the Thomson cross section and $U_B = B^2/8\pi$, the magnetic field density. The dependence on

m^{-2} shows that in general the synchrotron emission from electrons will be much stronger than from protons ($m_p \sim 2 \cdot 10^3\, m_e$).

In the relativistic case of charges moving with a substantial fraction of the speed of light there are two major effects which have to be taken into account:

- **Relativistic beaming:** The relativistic Doppler effect affects the observed flux density S_ν (arriving energy per unit area and unit frequency) from a source which moves relativistically with a component of velocity towards or away from the observer $\beta_{||}$ emitting the flux density S'_ν in the comoving frame (e.g. Rybicki & Lightman 1979).

  $$S_\nu = D^3 S'_\nu \tag{2.4}$$

  with the Doppler factor defined by

  $$D = \frac{1}{\gamma(1 - \beta_{||} \cos\Theta)} \quad . \tag{2.5}$$

  Although this dependence on the angle of the emitter velocity to the line of sight is reduced to $D^{2-\alpha}$ for a continuous jet with spectral index α, the amplification (or reduction) of an approaching (or receding) source can be dramatic. An intrinsically isotropically emitted radiation is beamed into a cone with the half opening angle $1/\gamma$ making its apparent luminosity strongly dependent on the angle it is viewed from.

- **The lighthouse effect:** The former effect implies that the radiation from a relativistically gyrating charge in a magnetic field can only be observed in a short pulse when (and if) the beaming cone of the moving charge on its way around the magnetic field line crosses the line of sight. A short calculation reveals the pulse to be of the length $\Delta T = \gamma^3 \omega_B \sin\alpha$. A Fourier analysis shows that a short pulse is always composed out of a wide range of frequencies up to $1/\Delta T$. For this reason, a charge which gyrates with a single discrete frequency around magnetic field line emits in a wide waveband around a characteristic frequency of

  $$\nu_c = 1\,\mathrm{MHz} \cdot \gamma^2 \left(\frac{B}{1\,G}\right) \tag{2.6}$$

  for a mean pitch angle of 30°.

2.1.2 Spectral distribution

In nature, there are usually ensembles of electrons, large numbers of particles with a certain energy distribution, involved in physical processes rather than single electrons of fixed energy. In the case of jets, it is usually assumed that this distribution corresponds to a power-law between two energy values E_1 and E_2.

$$N(\gamma)d\gamma = N_0 \cdot \gamma^{-s} d\gamma \tag{2.7}$$

An ensemble of electrons with a power-law energy distribution in the presence of a magnetic field emits a continuous spectrum of synchrotron radiation which has again the spectral shape of a power-law:

$$S_\nu \propto \nu^\alpha \quad . \tag{2.8}$$

Indeed this is the typical shape of many classes of radio sources[1]. In this case the energy distribution of the electrons in the source can be derived:

$$\alpha = \frac{1-s}{2} \quad \Rightarrow \quad s = 1 - 2\alpha \tag{2.9}$$

The radio lobes of Cygnus A, for example, show a spectral index α of ~ -0.8 indicating an energy distribution of $s = 2.6$. The spectrum of a synchrotron source can usually be described by a single power–law above a specific frequency ν_t. Below ν_t the spectrum typically falls of, which indicates the start of an absorption mechanism at lower frequencies. ν_t is called the turnover frequency. The next section describes the two most important absorption mechanisms with respect to AGN spectra.

2.1.3 The SSC mechanism

Based on the compactness of the features observed in extragalactic jets by VLBI (often unresolved at milliarcsecond–scales) and on the observation of intra–day variability, indicating emitting regions of the order of lightdays, there is evidence that Compton scattering processes are at work in AGN. It is rather an open question of whether this effect contributes a substantial fraction of the high energy emission (e.g. in the X-ray regime) observed in many sources (or are even the main contributor of such photons) or if these processes are negligible. There are other processes which can produce high energy photons, such as thermal bremsstrahlung of hot gas (possibly of an ADAF–like accretion flow), but there always have to be high energy photons originating in a Compton scattering event of lower energy photons at high energy particles.

The SSC (Synchrotron Self Compton) mechanism is the special case of inverse Compton scattering where synchrotron photons scatter off the very same electrons which produced them. 'Inverse' means that the radio photons gain energy in this event from the electrons and are upscattered to higher frequencies. In this model the inverse Compton spectrum should mimic the synchrotron spectrum in a different wavelength regime. Assuming a simple homogeneous sphere model for a component in a radio jet and deriving the jet parameters from VLBI observations it is possible to predict the SSC-scattered spectrum of the jet component. By adding up all the jet components (perhaps with a special consideration about the core component, for which a sphere is a poor approximation) a SSC-flux density can be obtained at every frequency to be compared with the measured flux density. The sum has to extend from the innermost component of a jet (depending on the considered frequency of the seed photons) out to the hot spots which will contribute a substantial fraction of the scattered flux in some cases.

It can be shown (e.g. Krolik 1999, section 9.2.1) that the luminosity of the inverse Compton radiation P_C relative to to the initial synchrotron luminosity P_S depends simply on the ratio of the energy density in the synchrotron photon field U_S and the magnetic field energy density U_B:

$$\frac{P_C}{P_S} = \frac{U_S}{U_B} \quad , \tag{2.10}$$

with $U_B = B^2/8\pi$. For a measured synchrotron flux density S_ν from a homogeneous

[1] With this definition of the spectral index α, negative values indicate a spectrum that falls towards higher frequencies. Sources with $-0.5 < \alpha < 0.5$ are usually called flat spectrum sources.

sphere with radius R the energy density of the photon field is

$$U_S = \frac{\text{Luminosity}}{\text{Proj.Area} \times \text{velocity}} = \frac{S_\nu \nu 4\pi D^2}{4\pi R^2 c} = S_\nu \cdot \nu \frac{1}{c}\frac{D^2}{R^2} \quad . \tag{2.11}$$

If S_ν, R and D are measured and B can be estimated (see Section 2.4.1 and 2.4.3), the Compton luminosity can be predicted and compared to the measurements.

The frequency of the inverse Compton scattered photons ν' simply depends on the frequency of the seed photons ν and the Lorentz factor γ_e of the electrons responsible for the scattering (e.g. Rybicki & Lightman 1979)

$$\nu' \sim \gamma_e^2 \nu \quad . \tag{2.12}$$

Thus, in order to produce X-ray emission of 1 keV ($\hat{=}2.4 \cdot 10^{17}$ Hz) from seed photons of 22 GHz, high energy electrons with Lorentz factors $\gamma_e = 1600$ are needed. Since these are the same electrons which produce the seed photons, the inverse Compton spectrum will be a "high energy reflection" of the initial synchrotron spectrum. A more detailed calculation of the spectrum can be found in Rybicki & Lightman (1979).

2.2 Jets

In chapter 1.2 a pure phenomenological description of extragalactic radio jets was given, with the emphasis on the morphology and the huge range in astronomical scales on which jets arise. In this section the underlying physics of the jet phenomenon shall be discussed in more detail, although many things will only be superficially presented. Not every aspect of jet theory is completely understood at present, especially how jets are formed and accelerated.

The black hole paradigm is generally accepted at present to explain the enormous amounts of energy liberated on small scales. For this, it seems quite natural to search for a principle that permits the ejection of matter perpendicular to the accretion disk feeding the black hole. The ejecta have to contain high energy electrons and/or positrons, since the radiation of jets is convincingly ascribed to synchrotron radiation which predicts magnetic fields to be involved. A strong interaction with the circumnuclear medium is expected, since the matter density in the vicinity of a black hole has to be substantial. At the base of a jet absorption effects are expected, first due to self absorption of the jet radiation and second due to free-free absorption of the circumnuclear medium. This section shall throw light on those aspects of jet physics, used in later chapters of the work.

2.2.1 Jet formation and propagation

Astrophysical jets always seem to be associated with black holes, or more general, a very compact object, which appears to be the prerequisite of jet formation. The most plausible theory of jet formation deals with the formation of a toroidal magnetic field, building a channel for charged particles due to electromagnetic interaction. If this picture were true, human–built particle accelerators on earth would just pattern themselves on active galactic nuclei in forming a collimated beam of charged particles in toroidal electromagnetic fields. The basic idea how these toroidal magnetic fields could be formed in AGN is that the footpoints of existing magnetic field lines in an accretion disk should be frozen in the

rotating matter. As the matter is compressed in the accretion process the magnetic field densities should increase and the field lines should be wound up as their footpoints rotate around the disk axis.

Other mechanisms could also lead to an acceleration and collimation of particles away from a compact and very active region as gas pressure or radiative forces. A more detailed review of theories on jet formation can be found for example in Krolik (1999).

As a basis for further discussion the following picture shall be taken as a paradigm for the innermost region of a jet: Substantial particle acceleration takes place in the very vicinity of an accretion disk. The accelerated particles are collimated by magnetohydrodynamic forces and guided along a channel outwards the central region in both directions perpendicular to the disk. At a distance r_N a nozzle is formed and the jet flow becomes supersonic. Beyond this point the particles are (re–)accelerated by the conversion of bulk kinetic energy to internal particle energy γ_e, e.g. via shock formation, resulting in a particle energy distribution represented by a power law

$$N(\gamma_e) = N_0 \gamma_e^{-s} \quad , \tag{2.13}$$

within a range $[\gamma_1, \gamma_2]$ of Lorentz factors. The jet is confined by an ambient medium with steep pressure and density gradients along the jet axis. Its hydrodynamics are given by a stationary adiabatic flow satisfying Bernoulli's equation $(\vec{v} \cdot \nabla)\gamma_j p^{1/4} = 0$ (Daly & Marscher 1988) with p, the pressure of the flow. This implies that the opening angle and the jet Lorentz factor should vary in presence of pressure gradients of the ambient medium. Nevertheless, the jet geometry can be approximated by a conical expansion, with a transverse radius $R \propto r$ with a opening angle $\Phi = \arctan(R/r)$.

Often it is assumed that the kinetic energy density of the jet (carried by electrons and protons) is in equipartition with the magnetic energy density

$$U_{e+p} = k \cdot U_B, \quad \text{with} \quad k \lesssim 1 \tag{2.14}$$

with $U_B = B^2/8\pi$. Under this assumption it is possible to integrate over the particle density distribution from γ_1 to γ_2 to derive the total density n of relativistic particles in the jet. A detailed calculation (e.g. Falcke & Biermann 1995) predicts

$$B \propto r^{-1} \quad \text{and} \quad n \propto r^{-2} \tag{2.15}$$

for the equipartition case. As another conclusion of the equipartition assumption it is possible to quantify the constant of proportionality in equation (2.8):

$$S_\nu = \frac{840 \cdot k}{\ln(\gamma_2/\gamma_1)} \mathrm{Jy} \left(\frac{B}{\mathrm{mG}}\right)^{3.5} \left(\frac{R}{\mathrm{kpc}}\right)^{3} \left(\frac{D}{\mathrm{Gpc}}\right)^{-2} \left(\frac{\nu}{\mathrm{GHz}}\right)^{-\frac{1}{2}} \tag{2.16}$$

for $s = 2$ (power law index of the particle energy distribution) and

$$S_\nu = \frac{840 \cdot k(s-2)}{(\gamma_1^{2-s} - \gamma_2^{2-s})} \mathrm{Jy} \left(\frac{B}{\mathrm{mG}}\right)^{3.5} \left(\frac{R}{\mathrm{kpc}}\right)^{3} \left(\frac{D}{\mathrm{Gpc}}\right)^{-2} \left(\frac{\nu}{\mathrm{GHz}}\right)^{\frac{1-s}{2}} \tag{2.17}$$

for $s \neq 2$. Thus, the flux density at the frequency ν of a spherical synchrotron source with the radius R and the distance D is determined mainly by the magnetic field and the energy index and range of Lorentz factors in the particle population.

2.2.2 Jet emission

According to the jet model described in 2.2.1 and the theory of synchrotron radiation a jet can be represented as the sum of many infinite thin slices forming the jet cone, each emitting synchrotron radiation determined through the local magnetic field, the energy index and range of Lorentz factors of the particle population, the distance to the jet origin and the frequency. The sum should extend from an innermost slice where the optical depth $\tau_S = 1$ (see Section 2.4.3) to a farthest slice at the end of the jet. This situation applies to an observation with a telescope which has a poor resolution compared to the extend of the jet, i.e. where the jet appears unresolved. Equation (2.16) has to be integrated along the jet axis from $r_{\tau=1}$ to infinity in order to derive the whole jet spectrum. For this integration the volume of the emitting sphere in Equation (2.16) has to be replaced by $4\pi R^2 dr$, with $R = \sin\Phi r$ the radius of a slice at the distance r to the jet origin. After a small calculation one ends up with

$$S_{Jet} \propto \nu^{-0.5} r_{\tau=1}^{-0.5} \tag{2.18}$$

for $s = 2$. Once again assuming equipartition and neglecting external absorption it can be used that the $\tau = 1$ surface depends on the observing frequency as

$$r_{\tau=1} \propto \nu^{-1} \tag{2.19}$$

(but see Section 2.4.3 for a general expression) and the frequency dependence in the spectrum cancels out.

> **The interpretation of a jet as a series of synchrotron emitting slices naturally leads to a flat spectrum!**

Deviation of flatness can be attributed to changes in the particle energy distribution along the jet, for example particle acceleration, bulk acceleration or a non–conical geometry.

2.2.3 The core–shift

Images of pc–scale jets obtained with Very Long Baseline Interferometry often show a feature with the following properties:

- Very compact or even unresolved on milliarcsecond scales
- Relatively bright, i.e. contributing a substantial fraction to the total flux
- In one–sided jets typically at one end of the linear structure
- Flat spectrum

A feature that has at least the first two properties is usually called the core of the jet. This term is quite misleading as it should not be identified with the central engine but with the part of the jet where it becomes visible. The innermost part of a jet is always invisible due to synchrotron self–absorption, since the optical depth τ of the jet at this part is very high. Traveling outwards the optical depth decreases due to the transversal expansion of the jet. The core is the part of the jet where $\tau \sim 1$ is reached. The optical depth due to self–absorption τ_s depends on the observing frequency and so does the core

position. For this reason it is often not correct to align VLBI maps at different frequencies by matching the position of the strongest component. One has to account for possible frequency-dependent shifts of optically thick features like a jet-core. An examination of the component spectra is required as optically thin features are much better candidates for footpoints of frequency independent regions.

With this definition of a core, it is obvious that a double–sided source as NGC 1052 should have two cores, one for each jet. Both cores are expected at the innermost part of the corresponding jet with the true origin of the jet activity somewhere in between.

In general a jet becomes visible at the distance r_c from the central engine where the optical depth due to synchrotron self–absorption and external absorption $\tau = \tau_s + \tau_f = 1$. If both sides are affected asymmetrically by external absorption, as it is implied by the standard model, in a disk or torus around the central engine, the optical depth on each side is altered correspondingly and the cores appear at different distances from the central engine. These different distances contain information about the different contributions of external absorption. Additionally, the optical depth due to free-free absorption τ_f depends differently on frequency than τ_s does. So, an analysis of the core shift with frequency can further constrain the influences of external absorption on both jets.

NGC 1052 is a prime object for such a kind of analysis, because both jets are still visible at the highest frequencies and so, the high resolution gives a very good estimate of the central engine position. It is possible to deal with absolute core shifts with frequency rather than relative changes as in one–sided jets.

Synchrotron self–absorption and pressure gradients: An expanding jet, confined by a medium with pressure p can be described by its opening angle $\Phi = \arctan(R/r)$ and the magnetic field B and the particle density N in the jet, with

$$B = B_1(r_1/r)^m, \quad N = N_1(r_1/r)^n \tag{2.20}$$

where R is the diameter of the jet at distance r and B_1 and N_1 are the magnetic field and the particle density at $r_1 = 1\,\mathrm{pc}$. The optical depth due to synchrotron self–absorption τ_s is (e.g. Rybicki & Lightman 1979)

$$\tau_s(r) = C(\alpha) N_1 \left(\frac{e\delta B_1}{2\pi m_e}\right)^{\epsilon} \frac{\Phi_0}{r^{\epsilon m+n-1}\nu^{\epsilon+1}} \tag{2.21}$$

where m_e is the electron mass, $\epsilon = 3/2 - \alpha$, $\Phi_0 = \Phi \csc(\theta)$ the observed opening angle, θ the viewing angle, r the distance from the central engine, ν the observing frequency and δ the Doppler factor. $C(\alpha)$ is described in Blumenthal & Gould (1970) and can be evaluated for every intrinsic spectral index α. If there is no contribution of external absorption, the core can be described by setting τ_s to 1. Equation (2.21) gives for the core position

$$r_c[\mathrm{pc}] = C_1 \cdot \nu^{-1/k_r} \tag{2.22}$$

with

$$C_1 = B_1^{k_b/k_r}(1+z)^{-1}[6.2 \cdot 10^{18} C(\alpha)\delta^{\epsilon} N_1 \Phi_0]^{1/(\epsilon+1)}. \tag{2.23}$$

Here $k_b = (3-2\alpha)/(5-2\alpha)$, and the core–shift is parameterized via

$$k_r = ((3-2\alpha)m + 2n - 2)/(5-2\alpha). \tag{2.24}$$

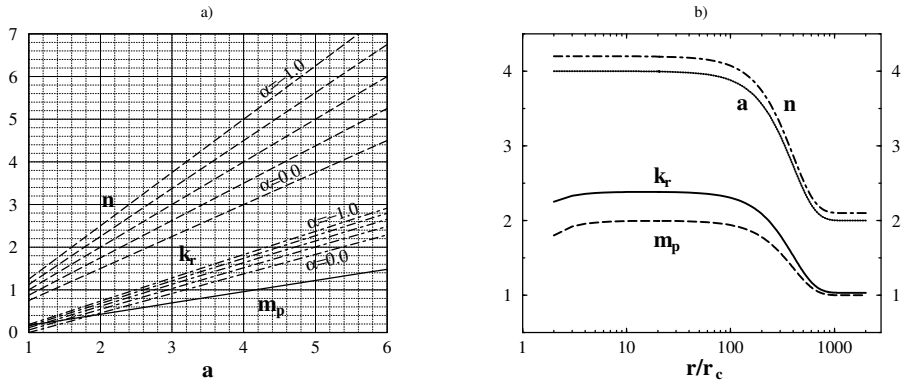

Figure 2.1: a) Dependence of n, m_p and k_r on pressure gradients. m is set to 1 and n and k_r are shown for different values of spectral index α. b) Change of the physical conditions along the jet axis, r. A spheric symmetrical exponential decrease of the pressure is assumed, $p(r) = p_0 \exp(-r^2/d^2)$. The medium extends to $400\, r_N$. k_r exhibits the largest deviations from its equipartition value of 1 at scales smaller than $100\, r_N$. Taken from Lobanov (1998).

Equation (2.22) predicts a linear relation between the logarithms of r_c and ν if m and n remain constant along the jet, i.e. if there are no pressure gradients. The slope of this relation is determined via Equation (2.24).

$$\log(r_c) \propto -\frac{1}{k_r} \cdot \log(\nu) \tag{2.25}$$

It can be shown (e.g. Falcke & Biermann 1995) that in the equipartition case $k_r = 1$. So, the task is to measure r_c at different frequencies and determine k_r via (2.24). Deviations from 1 then have to be attributed to pressure gradients in a confining medium. In the presence of steep pressure gradients, the Doppler factor and opening angle of the jet will vary in order to fulfill Bernoulli's equation and so will m and n (Georganopoulos & Marscher 1996) which determine the gradients of B and N, respectively. If the pressure varies as $p \propto r^{-a}$ then $m \rightarrow m_p = a/4m$ and $n = a(3 - 2\alpha)/4$. Figure 2.1 a (taken from Lobanov 1998) shows the dependence of magnetic field and particle density gradients on the pressure gradients of the ambient medium. In a more realistic model, the pressure density falls exponentially

$$p(r) = p_0 e^{-r^2/d^2}, \tag{2.26}$$

with a characteristic distance d from the central engine. This pressure gradient is more likely to be appropriate to model either a smooth medium like a torus or a cloudy one, maybe the same as the broad line region indicated by optical studies of AGN. In this case an approximation with a power–law is only useful with a variable power law index $a = a(r)$. Lobanov (1998) calculated the dependence of a, n, m_p and k_r along r in such a system with $d = 400 r_N$, $m = 2$ and $a(r_c) = 4$, with r_N the distance from the central engine to the location where the flow becomes supersonic (see Figure 2.1b). It is obvious that k_r does not exceed values of 2.5 for reasonable power–law indices a of the pressure. Higher values of k_r, i.e., smaller core shifts than $\propto \nu^{-0.4}$ can not be attributed to synchrotron self–absorption.

External absorption: The optical depth of a jet region can be altered from its intrinsic value due to synchrotron self–absorption if the foreground medium causes external

absorption. This absorber can be located anywhere between the observer and the source but especially a circumnuclear medium, possibly with a disk-like or toroidal shape, can contribute significantly to the optical depth. In this case, one expects the medium to be ionized from the central source causing free-free absorption. In the general case $\tau = \tau_s + \tau_f$, with τ_f the optical depth due to free-free absorption.

Observations of Cyg A (Krichbaum et al. 1998), Cen A (Jones et al. 1996) and also NGC 1052 (Kellermann et al. 1999) suggest a free–free absorbing torus around the nucleus of an AGN perpendicular to the jet axis. If this is inclined by a moderate angle to the line of sight of the observer, the counterjet is obscured with the strongest absorption at its core. Depending on the geometry of the system, a smaller fraction of the jet can also be covered by the absorber if the torus extends sufficiently high above the accretion disk plane. Another possibility would be a cloudy medium like the broad line region (BLR) formed of hydrogen plasma clouds. The optical depth due to free-free absorption is given by (see Levinson et al. 1995)

$$\tau_f(r) = \int_L 5 \cdot 10^{16} T^{-1.5} \nu^{-2} \bar{g} n_e(r) n_i(r) dl \quad , \tag{2.27}$$

where L is the length of the absorbing path in units of pc and dl a line element along this path. T is the temperature of the absorber, n_e and n_i the electron and ion density, respectively, and $\bar{g}$ is the hydrogenic gaunt factor. The latter can be written as $\bar{g} \sim 5.99 \cdot T^{0.15} \nu^{-0.1}$ (e.g. Brown 1987). If we assume a pure hydrogen plasma and a power–law decrease of the density, we can set $n_e(r) = n_i(r) = n_0 r^{-n}$ and equation (2.27) becomes

$$\tau_f(r) \sim 30 \cdot 10^{16} \int_L T^{-1.35} \nu^{-2.1} n_0^2 r^{-2n} dl \tag{2.28}$$

In the scenario of an initially optically thin region of the jet, which becomes optically thick only due to free-free absorption, this expression has to be set to 1. In general, a special model has to be developed to solve for the dependence of r on l. To the first order, r can be set to be independent of l and $\int_L dl = L$. In this case $\tau_f \propto \nu^{-2.1} r^{-2n}$ and values of $n \leq 4$ (comparable to the ones used in the example in Figure 2.1) lead to

$$r_c \propto \nu^{-0.25} \Rightarrow k_r = 4, \tag{2.29}$$

a value much higher than possible without external absorption effects. In this simple model the value of k_r is a direct measure of the density gradient at the core position. The analysis of core–shifts in jets therefore is capable to distinguish between internal and external absorption, if the crucial parameter k_r is determined to a value larger than 2.5. The combination of spectral– and core–shift analysis can even constrain the density gradients of an external absorber or the confining medium of the jet, respectively.

Bibliography

Barth, A. J., Filippenko, A. V., & Moran, E. C. 1999, Astrophys. J., 515, L61

Becklin, E. E., Tokunaga, A. T., & Wynn-Williams, C. G. 1982, Astrophys. J., 263, 624

Blandford, R. D. & Königl, A. 1979, Astrophys. J., 232, 34

Blumenthal, G. R. & Gould, R. J. 1970, Reviews of Modern Physics, 42, 237

Braatz, J. A., Wilson, A. S., & Henkel, C. 1996, Astrophys. J. Suppl., 106, 51

Brown, R. L. 1987, in Spectroscopy of Astrophysical Plasmas, 35–58

California Institute of Technology. 1991, BAAS, 23, 991

Claussen, M. J., Diamond, P. J., Braatz, J. A., Wilson, A. S., & Henkel, C. 1998, Astrophys. J., 500, L129

Condon, J. J., Condon, M. A., Gisler, G., & Puschell, J. J. 1982, Astrophys. J., 252, 102

Daly, R. A. & Marscher, A. P. 1988, Astrophys. J., 334, 539

de Vries, W. H., Barthel, P. D., & O'Dea, C. P. 1997, Astron. & Astrophys., 321, 105

Eckart, A. & Genzel, R. 1996, Nature, 383, 415

Falcke, H. & Biermann, P. L. 1995, Astron. & Astrophys., 293, 665

Falcke, H., Wilson, A. S., & Simpson, C. 1998, Astrophys. J., 502, 199

Fomalont, E. 1981, Newsletter. NRAO No. 3, p. 3, 1981, 3, 3

Forbes, D. A., Georgakakis, A. E., & Brodie, J. P. 2001, Monthly Not. Roy. Astron. Soc., 325, 1431

Fosbury, R. A. E., Mebold, U., Goss, W. M., & Dopita, M. A. 1978, Monthly Not. Roy. Astron. Soc., 183, 549

Gómez, J. L., Marscher, A. P., Alberdi, A., Jorstad, S. G., & García-Miró, C. 2000, Science, 289, 2317

Gabel, J. R., Bruhweiler, F. C., Crenshaw, D. M., Kraemer, S. B., & Miskey, C. L. 2000, Astrophys. J., 532, 883

Gallagher, J. S. 1986, Publ. Astron. Soc. Pacific, 98, 81

Georganopoulos, M. & Marscher, A. P. 1996, in ASP Conf. Ser. 100: Energy Transport in Radio Galaxies and Quasars, 67

Guainazzi, M. & Antonelli, L. A. 1999, Monthly Not. Roy. Astron. Soc., 304, L15

Guainazzi, M., Oosterbroek, T., Antonelli, L. A., & Matt, G. 2000, Astron. & Astrophys., 364, L80

Harris, D. E., Carilli, C. L., & Perley, R. A. 1994, Nature, 367, 713

Harris, D. E. & Krawczynski, H. 2002, Astrophys. J., 565, 244

Heeschen, D. S. 1970, Astron. J., 75, 523

Heeschen, D. S. & Puschell, J. J. 1983, Astrophys. J., 267, L11

Ho, L. C., Filippenko, A. V., & Sargent, W. L. 1995, Astrophys. J. Suppl., 98, 477

Ho, L. C., Filippenko, A. V., & Sargent, W. L. W. 1997, Astrophys. J. Suppl., 112, 315

Högbom, J. A. 1983, in Indirect Imaging. Measurement and Processing for Indirect Imaging. Proceedings of an International Symposium held in Sydney, Australia, August 30-September 2, 1983. Editor, J.A. Roberts; Publisher, Cambridge, England, New York, USA, Cambridge University Press, 1984, 247

Johnston, K. J., Fey, A. L., Zacharias, N., Russell, J. L., Ma, C., de Vegt, C., Reynolds, J. E., Jauncey, D. L., Archinal, B. A., Carter, M. S., Corbin, T. E., Eubanks, T. M., Florkowski, D. R., Hall, D. M., McCarthy, D. D., McCulloch, P. M., King, E. A., Nicolson, G., & Shaffer, D. B. 1995, Astron. J., 110, 880

Jones, D. L., Tingay, S. J., Murphy, D. W., Meier, D. L., Jauncey, D. L., Reynolds, J. E., Tzioumis, A. K., Preston, R. A., McCulloch, P. M., Costa, M. E., Kemball, A. J., Nicolson, G. D., Quick, J. F. H., King, E. A., Lovell, J. E. J., Clay, R. W., Ferris, R. H., Gough, R. G., Sinclair, M. W., Ellingsen, S. P., Edwards, P. G., Jones, P. A., van Ommen, T. D., Harbison, P., & Migenes, V. 1996, Astrophys. J., 466, L63

Jones, D. L., Wehrle, A. E., Meier, D. L., & Piner, B. G. 2000, Astrophys. J., 534, 165

Jones, D. L., Wrobel, J. M., & Shaffer, D. B. 1984, Astrophys. J., 276, 480

Kameno, S., Sawada-Satoh, S., Inoue, M., Shen, Z., & Wajima, K. 2001, Publ. Astron. Soc. Japan, 53, 169

Kellermann, K. I., Vermeulen, R. C., Cohen, M. H., & Zensus, J. A. 1999, in American Astronomical Society Meeting, Vol. 194, #20.02

Kellermann, K. I., Vermeulen, R. C., Zensus, J. A., & Cohen, M. H. 1998, Astron. J., 115, 1295

Kemball, A. J., Diamond, P. J., & Cotton, W. D. 1995, Astron. &. Astrophys. Suppl., 110, 383

Knapp, G. R., Faber, S. M., & Gallagher, J. S. 1978, Astron. J., 83, 139

Krichbaum, T. P., Alef, W., Witzel, A., Zensus, J. A., Booth, R. S., Greve, A., & Rogers, A. E. E. 1998, Astron. & Astrophys., 329, 873

Krolik, J. H. 1999, Active galactic nuclei : from the central black hole to the galactic environment (Princeton, NJ, USA : Princeton University Press, 1999.)

Leppänen, K. J., Zensus, J. A., & Diamond, P. J. 1995, Astron. J., 110, 2479

Levinson, A., Laor, A., & Vermeulen, R. C. 1995, Astrophys. J., 448, 589+

Lobanov, A. P. 1998, Astron. & Astrophys., 330, 79

Marr, J. M., Taylor, G. B., & Crawford, F. 2000, in Astrophysical Phenomena Revealed by Space VLBI, Proceedings of the VSOP Symposium, held at the Institute of Space and astronautical Science, Sagamihara, Kanagawa, Japan, January 19 - 21, 2000, Eds.: H. Hirabayashi, P.G. Edwards, and D.W. Murphy, Sagamihara, Kanagawa, Japan: Institute of Space and astronautical Science, 2000, 91

Mayall, N. U. 1939, Lick Observatory Bulletin, 497, 33

McDowell, J. C. 1994, in Einstein Obs. Unscreened IPC Data Archive

Mirabel, I. F. & Rodríguez, L. F. 1999, Annu. Rev. Astron. Astrophys., 37, 409

Miyoshi, M., Moran, J., Herrnstein, J., Greenhill, L., Nakai, N., Diamond, P., & Inoue, M. 1995, Nature, 373, 127

Napier, P. J. 1994, in IAU Symp. 158: Very High Angular Resolution Imaging, Vol. 158, 117

Omar, A., Anantharamaiah, K. R., Rupen, M., & Rigby, J. 2002, Astron. & Astrophys., 381, L29

Pearson, T. J., Shepherd, M. C., Taylor, G. B., & Myers, S. T. 1994, in American Astronomical Society Meeting, Vol. 185, #08.08

Peterson, B. M. 1997, An introduction to active galactic nuclei (Cambridge, UK, New York, USA: Cambridge University Press)

Pogge, R. W., Maoz, D., Ho, L. C., & Eracleous, M. 2000, Astrophys. J., 532, 323

Ros, E. 1997, Astrometría diferencial de precisión con VLBI en el triángulo de Draco (y estudios de SN 1993J) (València, Spain: Servicio de Publicaciones, Universitat de València), 35

Rybicki, G. B. & Lightman, A. P. 1979, Radiative Processes in Astrophysics (New York, USA: Wiley-Interscience)

Schwartz, D. A., Marshall, H. L., Lovell, J. E. J., Piner, B. G., Tingay, S. J., Birkinshaw, M., Chartas, G., Elvis, M., Feigelson, E. D., Ghosh, K. K., Harris, D. E., Hirabayashi, H., Hooper, E. J., Jauncey, D. L., Lanzetta, K. M., Mathur, S., Preston, R. A., Tucker, W. H., Virani, S., Wilkes, B., & Worrall, D. M. 2000, Astrophys. J., 540, L69

Smith, D. A., Wilson, A. S., Arnaud, K. A., Terashima, Y., & Young, A. J. 2002, Astrophys. J., 565, 195

Thompson, A. R., Moran, J. M., & Swenson, G. W. 1986, Interferometry and synthesis in radio astronomy (New York, Wiley-Interscience)

Tingay, S. J. & Murphy, D. W. 2001, Astrophys. J., 546, 210

Van Gorkom, J. H., Knapp, G. R., Raimond, E., Faber, S. M., & Gallagher, J. S. 1986, Astron. J., 91, 791

Vermeulen, R. C., Readhead, A. C. S., & Backer, D. C. 1994, Astrophys. J., 430, L41

Vermeulen, R. C., Ros, E., Kellermann, K. I., Cohen, M. H., & Zensus, J. A. 2002, in prep.

Wagner, S. J. & Witzel, A. 1995, Annu. Rev. Astron. Astrophys., 33, 163

Weaver, K. A., Wilson, A. S., Henkel, C., & Braatz, J. A. 1999, Astrophys. J., 520, 130

Wells, D. C., Greisen, E. W., & Harten, R. H. 1981, Astron. &. Astrophys. Suppl., 44, 363

Wilson, A. S. & Yang, Y. 2002, Astrophys. J., 568, 133

Wilson, A. S., Young, A. J., & Shopbell, P. L. 2000, Astrophys. J., 544, L27

Wrobel, J. M. 1984, Astrophys. J., 284, 531

Young, A. J., Wilson, A. S., Terashima, Y., Arnaud, K. A., & Smith, D. A. 2002, Astrophys. J., 564, 176

Yusef-Zadeh, F., Melia, F., & Wardle, M. 2000, Science, 287, 85

Zensus, J. A. 1997, Annu. Rev. Astron. Astrophys., 35, 607

Zensus, J. A., Ros, E., Kellermann, K. I., Cohen, M. H., Vermeulen, R. C., & Kadler, M. 2002, in press (Astron. J., issue August 2002)